College of Engineering

Methyltrimethoxysilane-insulated piezoelectric microcantilevers for direct, all-electrical biodetection in buffered aqueous solutions

Joseph A. Capobianco
Department of Materials Science and Engineering, Drexel University, Philadelphia, Pennsylvania 19104

Wan Y. Shih
School of Biomedical Engineering, Science, and Health Systems, Drexel University, Philadelphia, Pennsylvania 19104

Wei-Heng Shih
Department of Materials Science and Engineering, Drexel University, Philadelphia, Pennsylvania 19104

We have examined coating $(PbMg_{1/3}Nb_{2/3}O_3)_{0.63}-(PbTiO_3)_{0.37}$ (PMN-PT)/tin piezoelectric microcantilever sensors (PEMSs) with a thin methyltrimethoxysilane (MTMS) by a simple solution method to electrically insulate the PEMS for biodetection in phosphate buffered saline (PBS) solutions. The PMN-PT/tin PEMSs were constructed using PMN-PT freestanding films that exhibited an electric-field-enhanced giant piezoelectric coefficient. The insulation procedure involved spin coatings of MTMS followed by cross-linking in water, which yielded a coating layer of about 10 nm in thickness on the tin side of the PEMS. We showed that the MTMS-insulated PMN-PT/tin PEMSs were capable of electrical self-excitation and self-sensing with a stable resonance spectrum exhibiting a quality factor of $Q=50$ when submerged in $0.1M$ PBS solution. Direct, all-electrical, *in situ* detection of *Escherichia coli* O157:H7 at various concentrations was demonstrated at a flow rate of 0.5 ml/min. A MTMS-insulated PMN-PT/tin PEMS 725 μm long consisting of a 22-μm-thick PMN-PT layer and a 6-μm-thick tin layer exhibited a mass detection sensitivity $\Delta m/\Delta f = -3 \pm 2 \times 10^{-12}$ g/Hz and a concentration sensitivity of better than 100 cells/ml in less than 1 ml of liquid. © *2006 American Institute of Physics.* [DOI: 10.1063/1.2403113]

I. INTRODUCTION

Current biosensing technologies rely on fluorescence,[1,2] laser,[3] or fiber-optics-based methods,[4] quartz crystal microbalance,[5] electrochemical enzyme immunoassays,[6] amplification schemes such as polymerase chain reaction (PCR),[7–9] and binding to metal particles.[10] Most of the techniques are neither direct nor quantitative and are slow. They do not lend themselves to multiplexing and high throughput. Development of direct biosensing technologies relies heavily on silicon-based microcantilevers[11–15] due to their availability and ease of integration with existing silicon-based methodologies. However, silicon-based microcantilevers require complex external optical components for deflection detection and an external driver for actuation. In comparison, piezoelectric sensors use electrical means for detection, which allows the measurement system to be compact and portable. Current piezoelectric biosensors are based on quartz crystal microbalances[16] (QCMs) with a mass detection sensitivity of 10^{-8} g/Hz, about 10 000 times less sensitive than the silicon-based microcantilevers. Piezoelectric microcantilever sensor (PEMS) consisting of a highly piezoelectric layer such as lead zirconate titanate[17] (PZT) or lead magnesium niobate-lead titanate, $(PbMg_{1/3}Nb_{2/3}O_3)_{0.63}-(PbTiO_3)_{0.37}$ (PMN-PT),[18,19] bonded to a nonpiezoelectric layer such as tin is a new type of mass sensors that use electrical means for detection and can be miniaturized for better mass detection sensitivity.[20] For piezoelectric cantilevers, monitoring static

deflection is not practical as the deflection-induced piezoelectric voltage decays within a matter of 0.1 s due to the fact that the piezoelectric layer is not a perfect insulator.[21] It is, therefore, more appropriate to monitor shifts in resonance frequency for detection. However, a prerequisite for electrically monitoring resonance frequency shift *in situ* requires the PEMS to be insulated in a manner that allows for complete submersion in ionic buffers without shorting. After insulation, PEMS must also be immobilized with receptors for sensing applications. The challenge is to find a method of insulation that (1) does not require a thick layer so as not to degrade the mechanical performance of the PEMS and (2) can also accommodate the requirement of receptor immobilization. So far, thin ceramic layers such as MgO,[22] Al_2O_3,[23] Si_3N_4,[22] Ta_2O_5,[22] TiO_2,[22] $BaTiO_3$,[22] and $SrTiO_3$ (Ref. 22) have been demonstrated as effective insulation layers but they require high-vacuum chemical vapor deposition (CVD), which is expensive and slow. Although polymeric insulation coatings such as polyimides[24,25] and benzocyclobutene[26] (BCB) can be deposited by the wet solution method, to be effective they require a thickness of tens of microns, which is too thick for PEMS applications. Thinner polymeric layers such as parylene again require CVD.[27,28] Additional disadvantages of parylene include poor adhesion to the electrode surface[29] and difficulty for receptor immobilization.[27]

In this study, we have examined coating PMN-PT/tin PEMSs with a thin methyltrimethoxysilane (MTMS) layer

125105-2   Capobianco, Shih, and Shih

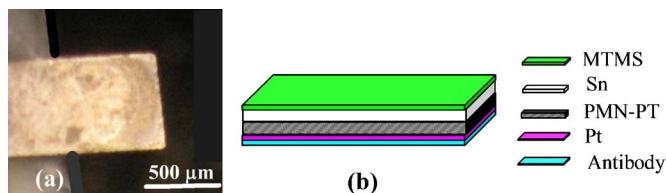Rev. Sci. Instrum. **77**, 125105 (2006)

FIG. 1. (Color online) (a) An optical micrograph of a typical PMN-PT/Sn PEMS viewed from the platinum side and (b) a schematic of the cross section of the PEMS.

FIG. 2. (Color online) In-air resonance spectrum of a 725-μm-long and 750-μm-wide PMN-PT microcantilever where the solid line, the dashed line, and the dash-dot-dot line represented the initial spectrum, the spectra after the first and second MTMS spin coatings, and the following cross-linking, respectively. The dashed vertical lines indicate the flexural-mode resonance frequencies calculated using the theory in Ref. 36. As can be seen the coating did not change the resonance peak heights or resonance peak widths much.

by a solution method to electrically insulate PMN-PT PEMS for in-water detection applications.[30] The PMN-PT/tin PEMSs were constructed from PMN-PT freestanding films that exhibited an electric-field-enhanced giant piezoelectric coefficient.[18] We showed that two spin coatings of MTMS followed by cross-linking in water yielded an insulating MTMS layer of about 10 nm that effectively insulated the PMN-PT/tin PEMSs. The solution deposition process was simple and the insulated PEMSs were used in the direct, electrical detection of *Escherichia coli* O157:H7 at various concentrations in a flow cell with better than 100 cells/ml concentration sensitivity with less than 1 ml of liquid.

II. EXPERIMENT

The PMN-PT/Sn PEMSs were constructed from freestanding PMN-PT films[18] of 22 μm in thickness. A 30-nm-thick nickel layer with a 15–30-nm-thick chromium/nickel bonding layer was first deposited on one side of the PMN-PT freestanding film by evaporation (E-gun Evaporator, Semicore Equipment, Livermore, CA) as the electrode. A 4-μm-thick tin layer was electroplated on the nickel surface at a rate of 500 nm/min as the nonpiezoelectric layer using a plating solution of tin sulfate titrated with sulfuric acid to a *p*H of 2.5. A 150-nm-thick platinum with a 10-nm-thick titanium bonding layer was evaporated on the other face of the film as the other electrode. The PMN-PT/Sn bilayer was then embedded in wax and cut to the cantilever shape with a wire saw (Princeton Scientific Precision, Princeton, NJ). After attaching the wires to the top and bottom electrodes using conductive glue (XCE 3104XL, Emerson and Cuming Company, Billerica, MA), the PMN-PT/Sn strips were finally glued to a glass substrate to form the microcantilevers.

To insulate the tin electrode of a PMN-PT/Sn PEMS, the PEMS was first soaked in a diluted (1:40 in water) piranha solution [two parts of 98% sulfuric acid (Fisher, Fair Lawn,
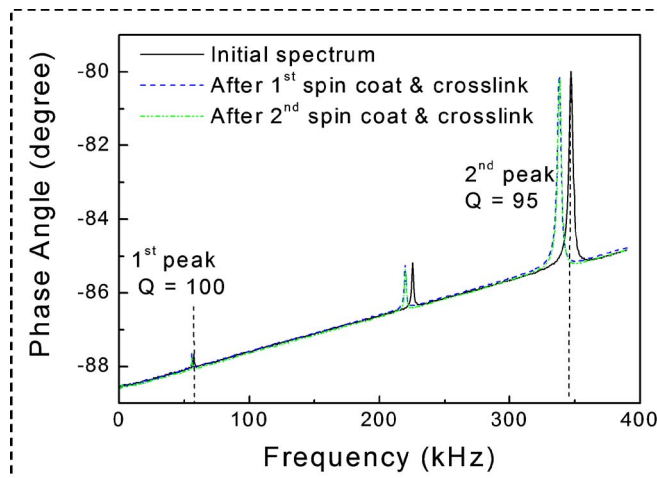
NJ) with one part of 30% hydrogen peroxide (FisherBiotech, Fair Lawn, NJ)] at 20 °C for 2 min to clean the tin surface. The oxidized tin surface was then treated with two MTMS (95% Aldrich, Milwaukee, WI) coatings for insulation. In each coating, the tin side of the PEMS was covered with MTMS for 1 min followed by spinning at 2500 rpm for 30 s (Photoresist Spinner, Headway Research Inc.). The PEMS was then soaked in de-ionized water overnight for cross-linking, followed by spinning at 2500 rpm for 30 s and overnight vacuum-oven (Model 1400E, VWR International) drying at 762 mm Hg. The above MTMS coating procedure was repeated one more time to have two MTMS coatings before the PEMS was used for in-water detection.

To demonstrate the in-water biodetection, antibodies were immobilized on the platinum surface of the PEMS. For antibody immobilization, the PEMS was first cleaned with a diluted (1:40 in water) piranha solution. After rinsing with de-ionized water, the PEMS was then submerged in a 2 mM aqueous solution of 3-mercaptopropionic acid (MPA) (99 +% Aldrich, St. Louis, MO) for 3 h for the sulfhydryl group of the MPA to attach to the platinum surface.[31–33] The carboxyl group of the immobilized MPA was then activated using a 5 mM aqueous solution of *N*-hydroxysuccinimide

TABLE I. Resonance frequency shifts and thickness of MTMS coatings on 5 MHz QCM.

	Initial frequency (Hz)	Frequency after first coat (Hz)	First coat Δf (Hz)	First coat thickness (nm)	Frequency after second coat (Hz)	Second coat Δf (Hz)	Second coat thickness (nm)	Total coating thickness (nm)
QCM #1	5 005 395	50 053 305	−65	3.9	5 005 277	−53	3.2	7.1
QCM #2	4 994 955	49 948 650	−90	5.4	4 994 796	−69	4.1	9.5
QCM #3	5 000 965	50 009 020	−63	3.8	5 000 845	−57	3.4	7.2
QCM #4	4 991 240	49 910 850	−155	9.3	4 991 056	−29	1.8	11
Average			−9.3	5.6		−52	3.1	8.7

Downloaded 09 Jan 2007 to 129.25.12.88. Redistribution subject to AIP license or copyright, see http://rsi.aip.org/rsi/copyright.jsp
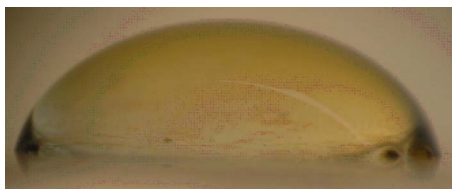
FIG. 3. (Color online) A photograph of a water droplet on the MTMS coating surface. The larger wetting angle evidenced that the MTMS coating with the methyl group converted the surface to a less hydrophilic one.

(NHS) (98% Aldrich, St. Louis, MO) and 1-ethyl-3-(3-dimethylaminopropyl)-carbodiimide (EDC) (Sigma, St. Louis, MO) for 30 min to be reactive to primary amines (lysine) in the antibody.[34–36] Finally, the PEMS was dipped in a 400 nM anti-*E. coli* O157:H7 antibody (Kirkegaard & Perry Laboratory, Gaithersburg, MD) in a phosphate buffered saline (PBS) solution (Sigma, St. Louis, MO). The heat killed *E. coli* O157:H7 was obtained from Kirkegaard & Perry Laboratory at Gaithersburg, MD.

III. RESULTS

A. Methyltrimethoxysilane coating

The microcantilever had a 22-μm-thick PMN-PT layer as the piezoelectric layer and a 6-μm-thick tin layer as the nonpiezoelectric layer and was 725 μm in length and 750 μm in width. An optical top view of the platinum side taken with stereomicroscope (SMZ-168, Motic, Richmond, British Columbia) and a schematic of the cross section of the PMN-PT/tin PEMS are respectively shown in Figs. 1(a) and 1(b). The initial resonance spectrum of a PMN-PT/tin microcantilever measured in air with an electrical impedance analyzer (Agilent 4294A, Agilent, Palo Alto, CA) before insulation is shown as a solid line in Fig. 2, which exhibited two flexural peaks with the first and second peaks at 57 and 347 kHz, respectively, as marked by the dashed vertical lines, which was calculated using the theory outlined in Ref.
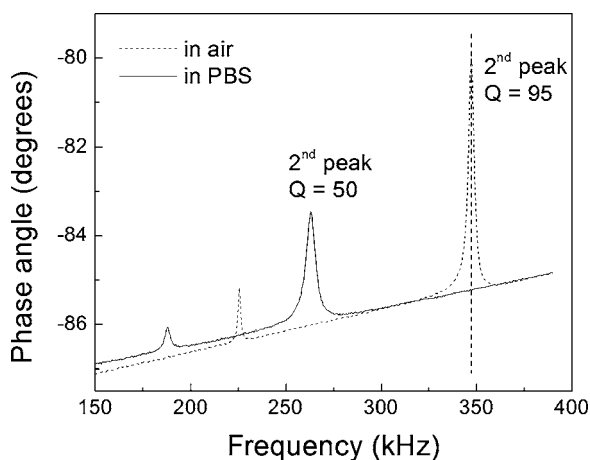

FIG. 4. Resonance spectrum of the MTMS-coated cantilever completely submerged in PBS (solid line). Also shown is the resonance spectrum of the MTMS-coated cantilever in air (dotted line) for comparison. The dashed vertical line indicates the flexural-mode resonance frequency in air using the theory in Ref. 36. As can be seen, upon submerging in PBS, the resonance peak height was reduced and the resonance peaks moved to lower frequencies.
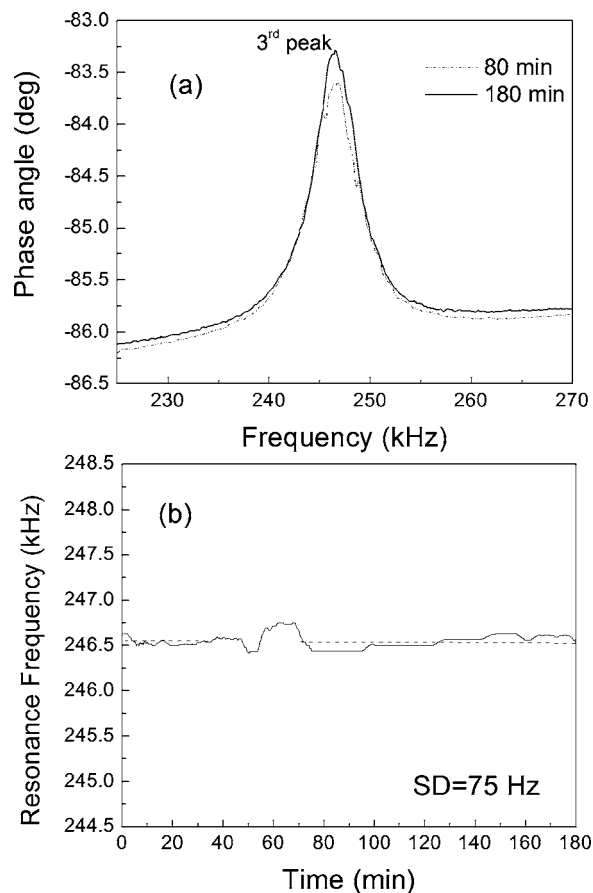

FIG. 5. (a) The in-PBS third-peak resonance spectra after 80 (dash-dot-dot line) and 180 (solid line) min in PBS and (b) the in-PBS third-peak resonance frequency vs time. As can be seen, the resonance spectrum was stable with time without degradation of the Q value (a) and the resonance frequency was stable with time with a standard deviation of 75 Hz.

37. The first and the second flexural-mode resonance peaks exhibited quality factors Q of about 100 and 95, respectively, where Q is defined as the ratio of the resonance frequency to the width of the resonance peak at half the peak height. The resonance spectra of the same cantilever in air after the first and second MTMS spin coatings and the following cross-linking are shown as the dashed line and dash-dot-dot line, respectively. The MTMS coatings did not seem to affect the in-air resonance peak height or peak width and the in-air Q values. The positions and widths of all resonance peaks remained close to their precoating values within error bars of 5 and 9 Hz, respectively.

A 5 MHz QCM (Stanford Research Systems, Sunnyvale, CA) was used to quantify the thickness of each MTMS coating layer. The gold electrode of the QCM was first cleaned with a piranha solution for 30 min followed by rinsing with de-ionized water and ethanol. The QCM was then soaked in a 40 mM solution of mercaptopropyltrimethoxysilane (MPS) (97% Alfa Aesar, Ward Hill, MA) in ethanol for 3 h and rinsed with ethanol. The QCM was then immediately soaked in 0.01M NaOH (99.99% Aldrich, Milwaukee, WI) for 48 h to facilitate hydrolysis and condensation. This procedure produced silanol and hydroxyl groups on the QCM surface to mimic the hydroxyl groups existed on the naturally oxidized tin surface. The QCM was subsequently rinsed with de-

ionized water. Upon completion of the process the resonance frequency was recorded using an impedance analyzer as the initial resonance frequency shown in Table I. After the MPS coating, MTMS was coated on the MPS-modified QCM surface as described in Sec. II. The resonance frequency after each coating was recorded and listed in Table I. From the resonance frequency shifts, Δf_{QCM}, the MTMS coating thickness was calculated using the following equation:[16]

$$\Delta t = -\frac{2f^2}{\sqrt{\mu_q/\rho_q}}\Delta f_{QCM},\tag{1}$$

where $f=5$ MHz was the natural resonance frequency of the QCM, and $\mu_q=2.947\times10^{11}$ dyn/cm^2 and $\rho=2.648$ g/cm^3 the shear modulus and density of the QCM, respectively. As can be seen from Table I, with four QCM measurements, the average thickness of the first and that of the second MTMS coating were 5.6 and 3.1 nm, respectively. The wetting angle of a water droplet on the MPS-modified QCM surface before the MTMS coatings (not shown) was 37°. After two coatings of MTMS, the surface became less hydrophilic (see Fig. 3) and the wetting angle became 69°.

After MTMS coating, the cantilever was then submerged in a PBS solution (Sigma, St. Louis, MO). The resonance spectrum of the MTMS-coated cantilever in PBS is shown in Fig. 4 as a solid line. Also shown is the spectrum of the same MTMS-coated cantilever taken in air (dotted line). As can be seen from Fig. 4, the cantilever retained two resonance peaks in PBS although both the resonance peak intensities and peak frequencies were lowered as a result of both the effect of liquid viscous damping and the mass of the liquid that moved with the cantilever.[38] Comparing the spectrum in PBS and that in air, one can see that the first flexural resonance peak disappeared in PBS, and the second flexural peak moved from 347 kHz with $Q=95$ to 263 kHz with a $Q=50$, indicating that the MTMS coatings electrically insulated the PMN-PT/tin microcantilever and maintained a good Q value. The stability of MTMS coating in PBS is shown in Figs. 5(a) and 5(b). Figure 5(a) shows the second flexural-mode resonance peak spectra of the PEMS in PBS at $t=80$ min (dash-dot-dot line) and 180 min (solid line) and Fig. 5(b) the second flexural-mode resonance frequency versus time. The spectra shown in Fig. 5(a) indicated that the resonance peak height was stable with time with no degradation of the Q values. Figure 5(b) shows that the resonance frequency remained stable with a standard deviation of about 75 Hz for the 3 h that the cantilever was monitored. These results indicated that the MTMS-coated cantilever can be used for detection in PBS as long as the detected frequency shift was larger than the standard deviation.

B. *E. coli* O157:H7 detection

For *E. coli* O157:H7 detection, the antibody-immobilized cantilever was immersed in a homebuilt flow cell[39] with a peristaltic pump (Model 77120-62, Cole-Parmer's Master Flex, Vernon Hills, IL). The flow cell contained 1 ml of *E. coli* suspension. The detection was carried out with the cantilever's two faces tangential to the flow at a flow rate of 0.5 ml/min for 30 min. After each detection, the
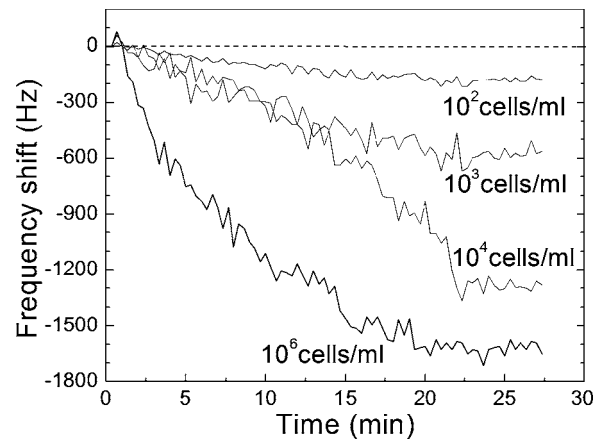

FIG. 6. Resonance frequency shift vs time during the detection of *E. coli* at various concentrations under the conditions of flow. Note that the large fluctuations in the resonance frequency shift at higher concentrations were signatures that the binding events were taking place, which was different from the relatively smaller fluctuations exhibited at lower concentrations and in pure PBS [Fig. 5(b)]. Using the MTMS insulation scheme the present PMN-PT/SnPEMS exhibited a better than 100 cell/ml concentration sensitivity for *in situ E. coli* detection by electrical means.

E. coli was released from the cantilever surface by flushing with a $pH=2.5$ glycine/HCl solution. Following the release with a $pH=2.5$ glycine/HCl solution, the PEMS was then exposed to an *E. coli* suspension of a different concentration ready for another detection. A MTMS-insulated PEMS could be reused for detection for five to six times by glycine/HCl release. After five to six detections, the PEMS can be regenerated by cleaning and reinsulation with MTMS. In Fig. 6, we plot the resonance frequency shift versus time obtained with *E. coli* suspensions of various concentrations. As can be seen, at 10^6, 10^4, 10^3, and 10^2 cells/ml, we obtained resonance frequency shifts of 1650, 1300, 600, and 200 Hz at $t=30$ min, respectively. Clearly, all resonance frequency shifts were well above the standard deviation of 75 Hz in PBS and the large resonance frequency shift correlated with a higher concentration. A summary of the resonance frequency shift at $t=30$ min versus concentration is shown in Fig. 7. Note that the present concentration detection limit of 100 cells/ml in less than 1 ml of liquid should be sufficient to detect *E. coli*
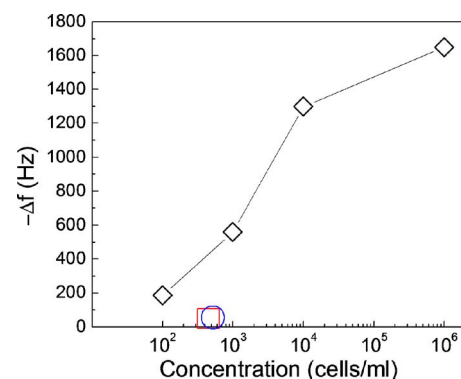

FIG. 7. (Color online) $-\Delta f_{30}$ vs concentration (open diamonds), where Δf_{30} was the resonance frequency shift at $t=30$ min. The open circle indicates the infection dosage (Ref. 40), and the open square indicates the concentration sensitivity of the commercial Raptor sensor which requires fluorescent labeling.

well below its infection dosage,[40] which is less than 700 cells/ml as marked by the open circle in Fig. 7. Also shown in Fig. 7 by the open square is the concentration sensitivity of commercial Raptors.[41] As can be seen, the present electrically insulated PEMS also exhibited better concentration sensitivity than the commercial Raptors. It is also worth noting that in addition to the sensitivity, the present PEMS was label-free and detected the cells directly from the suspension, while the commercial Raptors require fluorescent labeling.

IV. DISCUSSION

The resonance frequency of a cantilever is proportional to $(K/M_e)^{1/2}$, where K is the effective spring constant and M_e the effective mass of the cantilever. As such, during detection, the change in resonance frequency may be due to the mass loading effect and the effect of the spring constant change as[42]

$$\Delta f = \frac{f}{2M_e}\Delta m + \frac{f}{2K}\Delta K, \qquad (2)$$

where Δf and f denote the resonance frequency change and the resonance frequency of the cantilever, respectively, and Δm and ΔK the mass change and the effective spring constant change arising from the detection, respectively.

The mass change on the sensor surface was determined from the sensor surface scanning electron microscopy (SEM) micrographs after detection. For ease of SEM imaging, simulated sensor surfaces of identical gold surface immobilized with antibody using the identical procedures were prepared and exposed to *E. coli* suspensions of various concentrations under identical flow conditions as in the detection. The SEM images of the simulated sensor surfaces exposed to *E. coli* suspensions of 10^6 and 10^4 cell/ml concentrations for 30 min are shown in Figs. 8(a) and 8(b), respectively. By cell counting on the SEM images and by averaging over 320 cells and 2.3×10^4 μm^2 in area, we determined that the mass change per unit area on the sensor surface was $\Gamma = 1 \times 10^{-6}$ g/cm^2 after the exposure to the 10^6 cell/ml suspension for 30 min. With the dimension described above, we obtained $\Delta m = \Gamma Lw = 6 \times 10^{-9}$ g. With $\Delta f = -1650$ Hz after 30 min in 10^6 cells/ml, we obtained $\Delta m/\Delta f = (-3 \pm 2) \times 10^{-12}$ g/Hz. The same cell counting procedure was carried out over 1500 μm^2 for the surface exposed to a 10^4 cell/ml suspension and yielded $\Gamma = 4 \times 10^{-3}$ g/cm^2 and a mass sensitivity $\Delta m/\Delta f = (-2 \pm 2) \times 10^{-12}$ g/Hz. Although the coverage of the surface exposed to the 10^4 cell/ml suspension was much lower than that exposed to the 10^6 cell/ml suspension
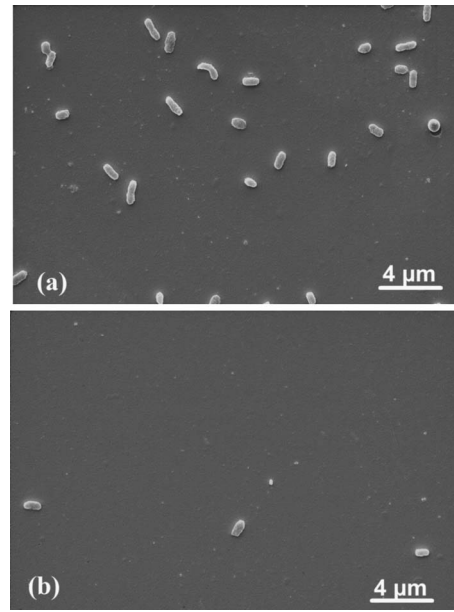

FIG. 8. SEM micrographs of *E. coli cells* captured on the simulated sensor surface after exposure to suspensions of (a) 10^6 cells/ml and (b) 10^4 cells/ml for 30 min. The area in both images is 875 μm^2. Note that in the images there is a small amount of residual salt from the saline buffer which could not be completely removed.

the obtained $(-2 \pm 2) \times 10^{-12}$ g/Hz mass detection sensitivity was consistent with the $(-3 \pm 2) \times 10^{-12}$ g/Hz obtained at 10^6 cells/Hz.

Note that this experimentally obtained $\Delta m/\Delta f$ was more than two orders of magnitude more sensitive than the predicted value when only the effect of mass loading is considered. Table II lists the various quantities involved in drawing the above conclusion. The quantity Γ is the surface coverage as determined from cell counting on the SEM micrographs discussed above, f the resonance frequency, $(\Delta f)_{ex}$ the experimental resonance frequency shift after 30 min of detection, $M_e = 0.234$ $(\rho_n t_n + \rho_p t_p)wL$ the effective mass of the PEMS,[43] $\Delta m = \Gamma wL$ the mass change due to the bound cells on the cantilever surface, $\Delta m/2M_e$ the relative mass change, $(\Delta f)_{\Delta m} = (f/2M_e)\Delta m$ the theoretical resonance frequency shift due to the mass change alone calculated from the first term on the right hand side of Eq. (2), and $\Delta K/K$ as deduced using $\Delta K/K = 2(\Delta f)_{ex}/f - (\Delta m)_{ex}/M_e$, where ρ_p and t_p (ρ_n and t_n) are the density and thickness of the PMN-PT (tin) layer, respectively, and w and L the width and length of the PEMS. As can be seen from Table II, the observed resonance frequency shifts were two orders of magnitude higher than what could be attributed to the mass-change effect alone.

TABLE II. Various quantities obtained after 30 min of detection at 10^6 and 10^4 cells/ml, where Γ is the surface coverage, f the resonance frequency, $(\Delta f)_{ex}$ the experimental resonance frequency shift, M_e the effective mass of the PEMS as defined in the text, Δm the experimental mass change as described in the text, $\Delta m/2Me$ the experimental relative mass change, $(\Delta f)_{\Delta m}$ the theoretical resonance frequency shift due to the mass change alone as calculated using the first term of the right hand side of Eq. (2), $(\delta f)_{ex}/f$ the experimental relative frequency shift, and $\Delta K/2K$ as deduced by $(\delta f)_{ex}/f - (\Delta m)_{ex}/2M_e$.

Concentration (cells/ml)	Γ (g/cm^2)	f (kHz)	$(\Delta f)_{ex}$ (Hz)	M_e (g)	Δm (g)	$\Delta m/2M_e$	$(\Delta f)_{\Delta m}$ (Hz)	$(\Delta f)_{ex}/f$	$\Delta K/2K$
10^6	1×10^{-6}	192	1650	2.64×10^{-5}	6×10^{-9}	1×10^{-4}	22	9×10^{-3}	9×10^{-3}
10^4	4×10^{-7}	192	1300	2.64×10^{-5}	2.6×10^{-5}	5×10^{-5}	10	7×10^{-3}	7×10^{-3}

Similar observations in other PEMS systems have been reported[17,44–46] and can be attributed to the second term on the right hand side of Eq. (2) involving ΔK, which has been shown to be related to the adsorption-induced surface stress.[42,44–46]

It is of interest to note that the fluctuations in the resonance frequency shift versus time appear to be part of the detection signals and not part of the instrumentation noise. This postulate is supported by the observation that the fluctuations diminish in pure PBS or in very low cell concentration and the amplitude of the fluctuations increases with increasing concentration (see Fig. 6). Similar fluctuations in resonance frequency shifts have also been observed in detections of other biological systems by piezoelectric microcantilevers.[19,39] Careful observations of the fluctuations in the resonance frequency shift may also serve as another "signature of detection" in addition to the absolute resonance frequency shift. However, to pinpoint the cause of the fluctuations would require more in-depth studies. We speculate that the fluctuations may be related to the antigen-antibody rearrangement on the sensor surface, which has been shown to result in binding stress relaxation, especially on a self-assembled monolayer[47] such as MPA which was used in the present sensor system. It could also be due to some of the temporary attachment and detachment of cells on the sensor surface in the suspension. It is, however, beyond the scope of this article to clarify the mechanism of these fluctuations.

In summary, the MTMS coating scheme examined in this study was able to electrically insulate the PMN-PT/tin PEMS and maintain a Q value of 50 in PBS for *in situ* all-electrical biodetection. The MTMS-insulated PMN-PT/tin PEMS 725 μm long, 750 μm wide exhibited a mass detection sensitivity of $(-3 \pm 2) \times 10^{-12}$ g/Hz and a concentration sensitivity of better than 100 cells/ml in less than 1 ml of liquid in *E. coli* detection.

ACKNOWLEDGMENTS

[1] S. Nie and R. N. Zare, Annu. Rev. Biophys. Biomol. Struct. **26**, 567 (1997).
[2] S. K. Kraeft *et al.*, Clin. Cancer Res. **10**, 3020 (2004).
[3] http://optics.org/articles/news/8/3/27/1
[4] R. T. Krivacic *et al.*, Proc. Natl. Acad. Sci. U.S.A. **101**, 10501 (2004).
[5] M. Minunni, M. Mascini, G. G. Guilbault, and B. Hock, Anal. Lett. **28**, 749 (1995).
[6] A. G. Gehring, D. L. Patterson, and S.-I. Tu, Anal. Biochem. **258**, 293 (1998).
[7] A. K. Bej, M. H. Mahbubani, M. J. Boyce, and R. M. Atlas, Appl. Environ. Microbiol. **60**, 368 (1994).
[8] B. A. Aback, S. J. O'day, and D. S. B. Hoon, Ann. N.Y. Acad. Sci. **1022**, 17 (2004).
[9] F. Oshita, A. Sekiyama, R. Suzuki, M. Ikehara, K. Yamada, H. Saito, K. Noda, and Y. Miyagi, Oncol. Rep. **10**, 105 (2003).
[10] S.-J. Park, T. A. Taton, and C. A. Mirkin, Science **295**, 1503 (2002).
[11] J. Fritz *et al.*, Science **288**, 316 (2000).
[12] A. Schemmel and H. E. Gaub, Rev. Sci. Instrum. **70**, 1313 (1999).
[13] D. R. Baselt, G. U. Lee, and R. J. Colton, J. Vac. Sci. Technol. B **14**, 798 (1996).
[14] G. U. Lee, D. A. Kidwell, and R. J. Colton, Langmuir **10**, 354 (1994).
[15] W. Han, S. M. Lindsay, and T. Jing, Appl. Phys. Lett. **69**, 4111 (1996).
[16] Z. Lin, C. M. Yip, I. S. Josheph, and M. D. Ward, Anal. Chem. **65**, 1546 (1993).
[17] Z. Shen, W. Y. Shih, and W.-H. Shih, Appl. Phys. Lett. **89**, 023506 (2006).
[18] H. Luo, Ph.D. thesis, Drexel University, Philadelphia, PA, 2005.
[19] W. Y. Shih, H. Luo, H. Li, C. Martorano, and W.-H. Shih, Appl. Phys. Lett. **89**, 242913 (2006).
[20] W. Y. Shih, W.-H. Shih, and Z. Shen, U.S. Patent Application No. PCT/US2004/036705 (October 27, 2004).
[21] S. T. Szewczyk, W. Y. Shih, and W.-H. Shih, Rev. Sci. Instrum. **77**, 044302 (2006).
[22] C. Bondoux, P. Prené, P. Belleville, F. Guillet, S. Lambert, B. Minot, and R. Jérisian, J. Eur. Ceram. Soc. **25**, 2795 (2005).
[23] P. Katiyar, C. Jin, and R. J. Narayan, Acta Mater. **53**, 2617 (2005).
[24] L. T. T. Nguyen, H. N. Nguyen, and T. H. T. La, Opt. Mater. (Amsterdam, Neth.) (in press).
[25] S. H. Cho, S. H. Kim, N.-E. Lee, H. M. Kim, and Y. W. Nam, Thin Solid Films **475**, 68 (2005).
[26] M. Ohnmacht, V. Seidemann, and S. Buttgenbach, Sens. Actuators, A **83**, 124 (2000).
[27] D. Feili, M. Schuettler, T. Doerge, S. Kammer, and T. Stieglitz, Sens. Actuators, A **120**, 101 (2005).
[28] K. S. Hwang, J. H. Lee, J. Park, D. S. Yoon, J. H. Park, and T. S. Kim, Lab Chip **4**, 547 (2004).
[29] A. Khabari and F. K. Urban III, J. Non-Cryst. Solids **351**, 3536 (2005).
[30] W. Y. Shih, J. Capobianco, and W.-H. Shih, U.S. Provision Patent Application No. 60/806,765 (July 7, 2006).
[31] D. B. Colin, E. B. Troughton, Y. T. Tao, J. Erall, M. W. George, and G. N. Ralph, J. Am. Chem. Soc. **111**, 321 (1989).
[32] M. Hasan, D. Bethell, and M. Brust, J. Am. Chem. Soc. **124**, 1132 (2002).
[33] C. Gutierrez-Wing, J. A. Ascencio, M. Perez-Alvarez, M. Marin-Almazo, and M. Jose-Yacaman, J. Cluster Sci. **9**, 529 (1998).
[34] Z. Grabarek and J. Gergely, Anal. Biochem. **185**, 131 (1990).
[35] D. G. Hoare and D. E. Koshland, Jr., J. Biol. Chem. **242**, 2447 (1967).
[36] L. A. Lyon, M. D. Musick, P. C. Smith, B. D. Reiss, D. J. Peña, and M. J. Natan, Sens. Actuators B **54**, 118 (1999).
[37] Z. Shen, W. Y. Shih, and W.-H. Shih, Rev. Sci. Instrum. **77**, 065101 (2006).
[38] W. Y. Shih, X. Li, H. Gu, W.-H. Shih, and I. A. Aksay, J. Appl. Phys. **89**, 1497 (2001).
[39] W. Y. Shih, W.-H. Shih, Z. Shen, Q. Zhu, J. Capobianco, and J. P. McGovern, U.S. provisional patent application No. 60/867,538 (November 6, 2006).
[40] J. Tuttle, T. Gomez, M. P. Doyle, J. G. Wells, T. Zhao, R. V. Tauxe, and P. M. Griffin, Epidemiol. Infect. **122**, 185 (1999).
[41] http://www.resrchintl.com/raptor.html
[42] G. Y. Chen, T. Thundat, E. A. Wachter, and R. J. Warmack, J. Appl. Phys. **77**, 3618 (1995).
[43] J. W. Yi, W. Y. Shih, R. Mutharasan, and W.-H. Shih, J. Appl. Phys. **93**, 619 (2003).
[44] J. H. Lee, K. S. Hwanga, J. Park, K. H. Yoon, D. S. Yoon, and T. S. Kim, Biosens. Bioelectron. **20**, 2157 (2005).
[45] H. Yoon, K. H. Yoon, K. H. Park, J. Ahn, and S. Kim, Biosens. Bioelectron. **20**, 269 (2004).
[46] J. H. Lee, T. S. Kim, and K. H. Yoon, Appl. Phys. Lett. **84**, 3187 (2004).
[47] R. Berger, E. Delamarche, H. P. Lang, C. Gerber, J. K. Gimzewski, E. Meyer, and H. J. Güntherodt, Science **276**, 2021 (1997).